Physical Understanding via Reduction of Complex Multiscale Models: Glycolysis in Saccharomyces cerevisiae

Panayotis D. Kourdis, Dimitris A. Goussis, Ralf Steuer

***Abstract*— We consider complex mathematical models that are characterized by a wide spectrum of time scales, the fastest of which are operative during the initial state only, leaving the slower ones to drive the system at later times. It is shown that very useful physical understanding can be acquired if the fast and slow dynamics are first separated and then analyzed. Existing algorithmic methodologies can be applied for this purpose. A demonstration of this approach is presented for a glycolysis model, the solution of which asymptotically evolves around a limit cycle.**

I. Introduction

The increasing complexity of the mathematical models in biology and genetics demand the development of algorithmic tools for the acquisition of the desired physical understanding [1]-[3].

For that purpose, a number of methodologies have been developed in order to construct reduced models that retain the significant features of the full model. Such algorithms have recently been employed successfully for the analysis of a large number of problems [4]-[11].

Reduction is mainly based on the development of very fast time scales, which quickly become exhausted, allowing slower scales to characterize the evolution of the physical process; i.e. they do not affect the progress of the system but they simply constrain its motion in a low dimensional space. This situation is usually defined as stiffness [12] and the low dimensional space, where the system evolves according to the slow time scales, is defined as a manifold [13]-[14].

Reduction algorithms on the basis of time scale gaps provide either both the manifold and the model governing the slow evolution [15]-[19] or simply the manifold [20]-[21]. These algorithms provide either leading order accuracy [17]-[18] or higher order accuracy in an iterative fashion [15]-[16], [19]-[21]; the measure of accuracy provided by the size of the gap between the fast and the slow time scales. Excellent reviews of such algorithms can be found in Refs. [22]-[23].

Here, the CSP algorithm [15]-[16] will be employed for the analysis of a model that describes the glycolysis of intact yeast cells as a *homogeneous* two-phase (intracellular/extracellular) system [24]-[25]. It will be shown that significant physical knowledge can be obtained by identifying the processes contributing the most to the fast and slow dynamics of the model; in particular here in the development of the manifold.

Manuscript received July 5, 2008. The authors PDK and DAG gratefully acknowledge the contribution of the NTUA basic research grant 65/1621.

P.D. Kourdis and D.A. Goussis are with the School of Applied Mathematics and Physics, National Technical University, 15773 Athens, Greece pkourdis@central.ntua.gr, dagoussi@mail.ntua.gr

R. Steuer is with the Manchester Interdisciplinary Biocentre, University of Manchester, Manchester, UK ralf.steuer@manchester.ac.uk

TABLE I
Reactions in the detailed model [24]

1	$\leftrightarrow Glc_x$
2	$Glc_x \leftrightarrow Glc$
3	$Glc + ATP \rightarrow G6P + ADP$
4	$G6P \leftrightarrow F6P$
5	$F6P + ATP \rightarrow FBP + ADP$
6	$FBP \leftrightarrow GAP + DHAP$
7	$DHAP \leftrightarrow GAP$
8	$GAP + NAD^+ \leftrightarrow BPG + NADH$
9	$BPG + ADP \leftrightarrow PEP + ATP$
10	$PEP + ADP \rightarrow Pyr + ATP$
11	$Pyr \rightarrow ACA$
12	$ACA + NADH \rightarrow EtOH + NAD^+$
13	$EtOH \leftrightarrow EtOH_x$
14	$EtOH_x \rightarrow$
15	$DHAP + NADH \rightarrow Glyc + NAD^+$
16	$Glyc \leftrightarrow Glyc_x$
17	$Glyc_x \rightarrow$
18	$ACA \leftrightarrow ACA_x$
19	$ACA_x \rightarrow$
20	$ACA_x + CN_x^- \rightarrow$
21	$\leftrightarrow CN_x^-$
22	$G6P + ATP \rightarrow ADP$
23	$ATP \rightarrow ADP$
24	$ATP + AMP \leftrightarrow 2\,ADP$

II. The Glycolysis Model

Oscillations in yeast glycolysis have been observed for several decades and models of the glycolytic pathway were developed since the 1960s. We focus on the full-scale model, developed by Hynne et al [24], that involves 24 reactions among 22 metabolites (see Table I). It is assumed that CSTR conditions prevail in which glucose, cyanide and a suspension of starved yeast cells flow into the reactor at a constant rate; the volume remaining fixed by removing the surplus liquid. Under these conditions, the governing equations are of the form:

$$\frac{d\mathbf{y}}{dt} = \mathbf{Q}^{-1}\left(\mathbf{S}_1 F^1 + ... + \mathbf{S}_N F^N\right) = \mathbf{g}(\mathbf{y}) \qquad (1)$$

where the elements of the N-dim. column vector $\mathbf{y}$ are the concentrations of the metabolites, the N-dim. column vector $\mathbf{S}_k$ and the scalar F^k denote the stoichiometric vector and rate, respectively, of the k-th reaction; N=22 for the model considered. The $N \times N$ matrix $\mathbf{Q}$ is diagonal, its entries equaling either unity for the intracellular metabolites or the

ratio of the extracellular volume to the total volume of intracellular cytosol, y_{vol}, for the extracellular ones. After an initial transient, system (1) exhibits a stationary or oscillatory (limit cycle) state, depending on the values of the parameters and the initial conditions.

Here the values of the parameters and ICs in [24] are employed; in particular the values of mixed flow glucose and cyanide concentrations $[Glc_x]_o = 24.0mM$ and $[CN_x^+]_o = 5.60mM$ and of the ratio $y_{vol} = 59$, for which the system eventually evolves well into the oscillatory state regime. This behavior is displayed in Figs. 1 and 2 for the evolution of concentration of intracellular acetaldehyde (ACA) and nicotinamide adenine dinucleotide (NADH); the behavior of the other metabolites being similar. It can easily be observed that the oscillatory motion is characterized by a frequency $\omega_{ch} = 2\pi/T = 10min^{-1}$, approximately.

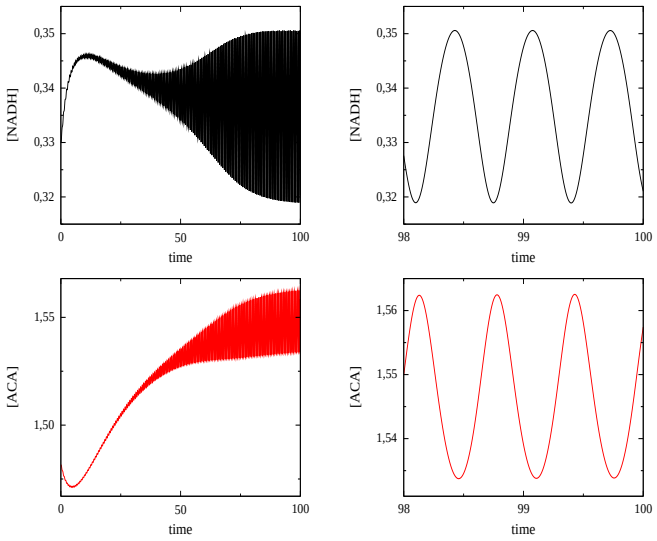

Fig. 1. The evolution of the NADH and ACA concentrations (mM) with time (min). On the right, magnification when fully oscillatory motion is established.

Fig. 2 shows that the oscillatory motion develops as various transient components die-out. As it is demonstrated in Fig. 3, fully oscillatory motion is established at sufficiently long times .

Along the trajectory past the initial transient, the rate of change of the concentration of various metabolites is much smaller than the magnitude of the reaction rates contributing to these rates of change. The magnitude of the occurring cancellations is demonstrated in Fig. 4 for the metabolites BPG and AMP, the governing equations of which are:

$$\frac{d[BPG]}{dt} = \left(R^{8f} - R^{8b}\right) - \left(R^{9f} - R^{9b}\right) \quad (2)$$

$$\frac{d[AMP]}{dt} = -\left(R^{24f} - R^{24b}\right) \quad (3)$$

where R^{kf} and R^{kb} denote the forward and backward rate of the k-th reaction, the expressions of which are taken

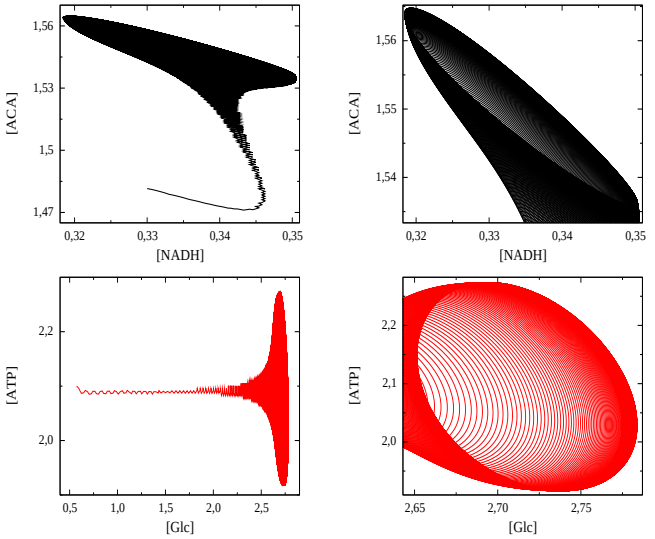

Fig. 2. The trajectory on the [NADH] - [ACA] and the [Glc] - [ATP] planes, during the period $0 < t < 150$ min. On the right, magnification in the region where fully oscillatory motion is established.

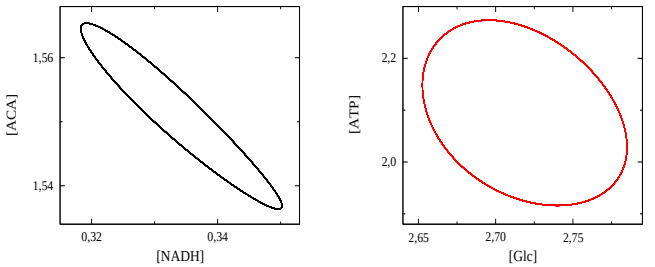

Fig. 3. The trajectory on the [NADH] - [ACA] and the [Glc] - [ATP] planes, during the period $450 < t < 500$ min.

from [24]. Comparing the magnitude of the reaction rates and that of the rate by which the concentrations change, Fig. 4 shows that significant cancellations are taking place among the forward and backward rates of Reactions 8 and 9 and of Reaction 24, resulting in a evolution of $[BPG]$ and $[AMP]$, respectively, much slower than that suggested by the magnitude of each of the rates involved.

Such cancellations are produced by the action of fast *dissipative* time scales, much faster than the characteristic ones of the system's behavior, in developing a number of equilibria (equal to the number of fast time scales) among various processes in the model that are mostly affected by these scales. The effect of these time scales in establishing equilibria and confining the evolution of the system within these equilibria becomes stronger as the gap with the characteristic (slower) time scales increases. Fast dissipative time scales relate to the largest in magnitude eigenvalues of the system's Jacobian, $\mathbf{J} = grad(\mathbf{g})$, the real part of which is negative and much larger than the imaginary part.

In the problem considered here, at each point in time the first 10 eigenvalues with the largest magnitude are real and

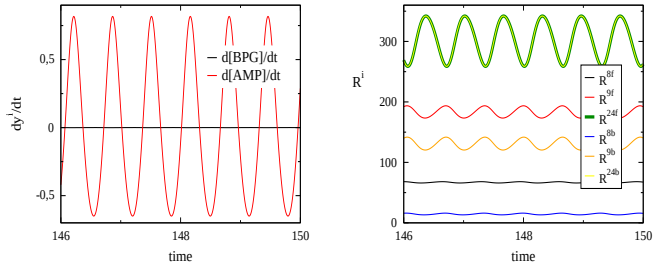

Fig. 4. The evolution of the rate of change of BPG and AMP concentrations (mM/min) with time (min) along with that of the related reaction rates.

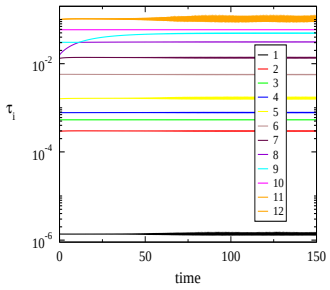

Fig. 6. The evolution in time (min) of the twelve fastest timescales.

negative; the next two forming a complex pair. The evolution of the real and imaginary parts of this eigenvalue pair is displayed in Fig. 5. It is shown that the imaginary part dominates the real part and is approximately equal to the frequency of the oscillatory motion, $\lambda_i = O(\omega_{ch} = 10min^{-1})$. Since the corresponding time scale can be considered as the characteristic of the system, these findings suggest that the maximum number of equilibria that can be established by fast dissipative time scales is ten.

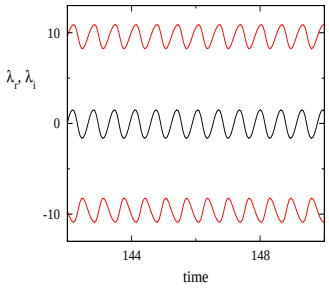

Fig. 5. The evolution in time (min) of the real (black) and imaginary (red) parts of the complex eigenvalue pair, $\lambda_{11,12} = \lambda_r \pm i\lambda_i$ (min^{-1}).

The k-th timescale is introduced here as:

$$\tau_k = \left(\sqrt{\lambda_{kr}^2 \ + \ \lambda_{ki}^2}\right)^{-1} \tag{4}$$

where the eigenvalue is defined as $\lambda_k = \lambda_{kr} + i\lambda_{ki}$; the subscripts "r" and "i" denoting real and imaginary parts, respectively. Fig. 6 displays the evolution of the twelve fastest time scales, where $\tau_{11} = \tau_{12}$ is considered the characteristic time scale of the system's evolution. It is shown that a large gap develops between τ_1 and τ_2; the gap between τ_{10} and τ_{11} being relatively small.

The usefulness of these fast time scales in producing a reduced model describing the slow oscillatory motion, see in Fig. 1, will be discussed next, after a brief presentation of the CSP method.

III. The CSP Method

According to the CSP method [15]-[16], [26]-[30], Eq. (1) is cast in the form:

$$\frac{d\mathbf{y}}{dt} = \mathbf{a}_1 f^1 + \mathbf{a}_2 f^2 + ... + \mathbf{a}_{N-1} f^{N-1} + \mathbf{a}_N f^N \tag{5}$$

where $\mathbf{a}_k$ and f^k denote the CSP basis N-dim. *column* vector and amplitude, respectively, of the k-th mode. The amplitudes are defined as:

$$f^k \ = \ \mathbf{b}^k \bullet \mathbf{g}(\mathbf{y}) \tag{6}$$

where the dual N-dim. *row* vectors $\mathbf{b}^k$ satisfy the orthogonality condition $\mathbf{b}^k \bullet \mathbf{a}_n = \delta_n^k$. Assuming that the M fastest time scales are of dissipative nature and are much faster than the rest, Eq. (5) can be cast as:

$$\frac{d\mathbf{y}}{dt} \ = \ \mathbf{a}_r \mathbf{f}^r \ + \ \mathbf{a}_s \mathbf{f}^s \tag{7}$$

where the terms $\mathbf{a}_r \mathbf{f}^r$ (fast modes) and $\mathbf{a}_s \mathbf{f}^s$ (slow modes) relate to the M fast and $K = N - M$ slow, respectively, time scales. The various quantities in Eq. (7) are defined as:

$$\mathbf{a}_r = \left(\begin{array}{ccc} \mathbf{a}_1 & .. & \mathbf{a}_M \end{array} \right) \quad \mathbf{b}^r = \left(\begin{array}{c} \mathbf{b}^1 \\ : \\ \mathbf{b}^M \end{array} \right) \tag{8}$$

$$\mathbf{a}_s = \left(\begin{array}{ccc} \mathbf{a}_{M+1} & .. & \mathbf{a}_N \end{array} \right) \quad \mathbf{b}^s = \left(\begin{array}{c} \mathbf{b}^{M+1} \\ : \\ \mathbf{b}^N \end{array} \right) \tag{9}$$

$$\mathbf{f}^r = \mathbf{b}^r \bullet \mathbf{g}(\mathbf{y}) = \left(\begin{array}{c} f^1 \\ : \\ f^M \end{array} \right) \tag{10}$$

$$\mathbf{f}^s = \mathbf{b}^s \bullet \mathbf{g}(\mathbf{y}) = \left(\begin{array}{c} f^{M+1} \\ : \\ f^N \end{array} \right) \tag{11}$$

When the fast *dissipative* times scales become exhausted, the corresponding amplitudes become negligibly small:

$$\mathbf{f}^r \approx \mathbf{0} \tag{12}$$

so Eq. (7) simplifies to:

$$\frac{d\mathbf{y}}{dt} \approx \mathbf{a}_s \mathbf{f}^s \tag{13}$$

denoting that the system evolves on a $N-M$-dim. manifold according to the slow time scales within the confines defined by the equilibration of the fast processes, Eq. (12); the later imposed by the action of the exhausted fast *dissipative* time scales. For the glycolysis model considered here, $N = 22$ and, as was discussed previously, $M_{max} = 10$.

The slow modes include the, so-called, conservation modes, which relate to infinitely slow time scales due to conservation laws; having no contribution to the system's evolution. For the glycolysis model considered here, there exist two conservation modes originating from the constraints $[NAD^+] + [NADG] = const$ and $[ATP] + [ADP] + [AMP] = const$. These modes produce the row vectors, say, $\mathbf{b}^{21}$ and $\mathbf{b}^{22}$, which produce $f^{21} \equiv 0$ and $f^{22} \equiv 0$. Such vectors are constructed as follows. The elements of $\mathbf{b}^{21}$ are all zero, except those which correspond to the concentrations $[NAD^+]$ and $[NADG]$, which are set equal to one. Similarly, the elements of $\mathbf{b}^{22}$ are all zero, except those which correspond to the concentrations $[ATP]$, $[ADP]$ and $[AMP]$, which are also set equal to one. In essence, these two conservation laws state that the detailed model, Eq. (1) evolves inside an - effectively - 20-dim. space.

The CSP basis vectors, $\mathbf{a}_k$ and $\mathbf{b}^k$, are computed using two iterative procedures [15]-[16]. The $\mathbf{b}^r$-refinement increases iteratively the accuracy by which the manifold, as expressed by Eq. (12), is approximated by increasing the accuracy of the set of basis vectors $\mathbf{b}^r$. Each $\mathbf{b}^r$-refinement yields:

$$\mathbf{f}^{k+1,r} = \epsilon\, \mathbf{f}^{k,r} \tag{14}$$

where $\mathbf{f}^{k,r} = \mathbf{b}^{k,r} \bullet \mathbf{g}(\mathbf{y})$ and $\epsilon = \tau_M/\tau_{M+1} < 1$ provides a measure of the fast/slow time scales gap [15]-[16], [28]. The $\mathbf{a}_r$-refinement guarantees that only slow time scales are encountered in the simplified model, Eq. (13); one such refinement being adequate [28]-[29].

Given that the simplified model is valid as long as the fast components are negligible, the M fast time scales are declared exhausted when:

$$\tau_{M+1}\mathbf{a}_r\mathbf{f}^r < \epsilon_{rel}\ \mathbf{y} + \epsilon_{abs} \tag{15}$$

where ϵ_{rel} and ϵ_{abs} denote the relative and absolute error allowed along a slow time step. It follows that the accuracy of simplified model Eq. (13) depends on both:

- the size of the gap among the fast and the slow time scale, as indicated by the magnitude of ϵ, and
- the number of $\mathbf{b}^r$-refinements employed.

Next, it will be demonstrated that the size of the reduced model is directly related to the desired accuracy, the fast/slow time scales gap and the number of $\mathbf{b}^r$-refinements employed.

IV. The Dimension of the Fast Subspace

Figs. 7, 8 and 9 show the evolution of the fast amplitudes, f^k where $k = 1, M$, for the cases $M = 6$, 8 and 10, respectively, when employing one and two $\mathbf{b}^r$-refinements.

In particular, Fig. 7 shows that when setting $M = 6$ a $O(10^{-2})$ error will be committed by rendering to the reduced model, if one $\mathbf{b}^r$-refinement is employed. This error reduces to $O(10^{-3})$, with an additional $\mathbf{b}^r$-refinement. Similarly, Fig. 8 shows that a $M = 8$ reduced model produces $O(10^{-1})$ and $O(10^{-2})$ errors when employing one and two, respectively $\mathbf{b}^r$-refinements. A somewhat smaller error reduction is produced by an additional $\mathbf{b}^r$-refinement for the $M = 10$ case, as shown in 9, the reduced model providing the most a $O(10^{-1})$ accuracy.

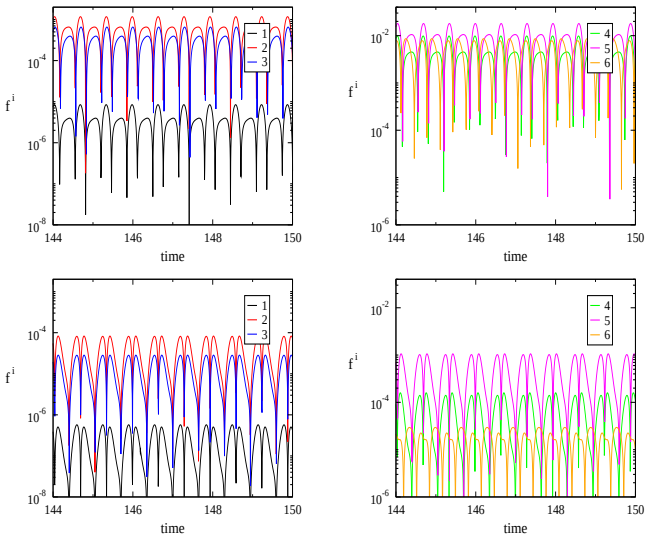

Fig. 7. M=6. The evolution in time (min) of the six fast CSP amplitudes; top: one $\mathbf{b}^r$-refinement, bottom: two $\mathbf{b}^r$-refinements.

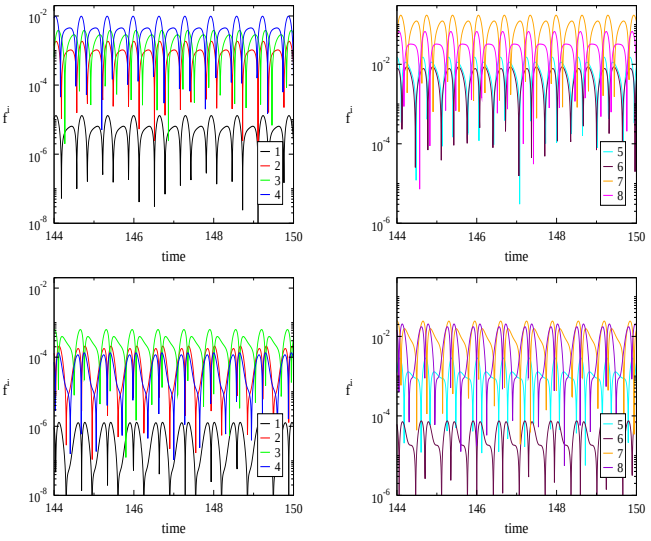

Fig. 8. M=8. The evolution in time (min) of the eight fast CSP amplitudes; top: one $\mathbf{b}^r$-refinement, bottom: two $\mathbf{b}^r$-refinements.

These findings are in very good agreement with the fact that the time scales gap in the three cases considered, $\epsilon_6 = \tau_6/\tau_7$, $\epsilon_8 = \tau_8/\tau_9$ and , $\epsilon_{10} = \tau_{10}/\tau_{11}$ are all about $O(10^{-1})$.

If one is interested in a $O(10^{-3})$ accuracy, the $M = 6$ reduced model seems adequate; the maximum reduction of $M = 10$ requiring more than two $\mathbf{b}^r$-refinements to meet this goal. In the following, the $M = 8$ case will be considered, which provides a $O(10^{-2})$ accuracy with only two $\mathbf{b}^r$-refinements; the reduced model constructed with an additional one $\mathbf{a}_r$-refinement.

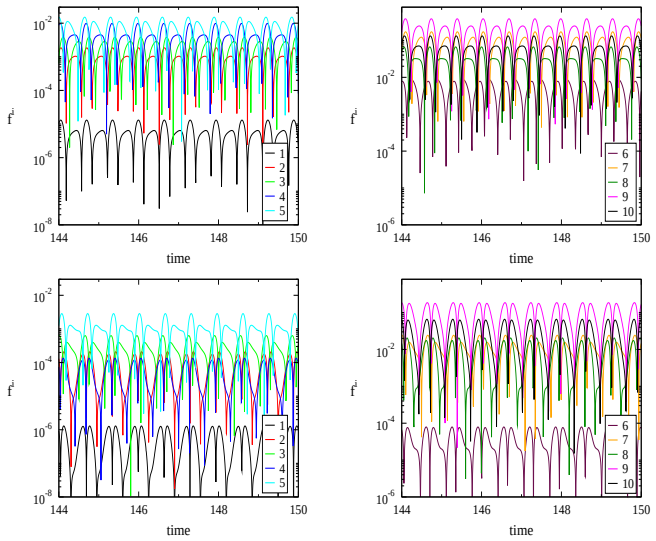

Fig. 9. M=10. The evolution in time (min) of the ten fast CSP amplitudes; top: one $\mathbf{b}^r$-refinement, bottom: two $\mathbf{b}^r$-refinements.

V. CSP Diagnostics on the Manifold

For the $M = 8$ case, the manifold is described by eight equations of the form:

$$f^k = \mathbf{b}^k \bullet \mathbf{g}(\mathbf{y}) = q^k_{1f}R^{1f} + .. + q^k_{24f}R^{24f} + q^k_{1b}R^{1b} + .. + q^k_{24b}R^{24b} \approx 0 \quad (16)$$

where the second equality follows from Eq. (1), $q^k_{if} = -q^k_{ib} = \mathbf{b}^k\mathbf{Q}^{-1}\mathbf{S}_i$ and $k = 1, M$. Each of these equations relates to a (usually small) number of variables, which are affected the most by the corresponding fast time scale and at the same time exhibit a strong influence to the terms participating in the occurring cancellations [27], [32]. These variables can be identified with the help of the CSP Pointer [26]-[27], [31]:

$$\mathbf{D}^k = diag\left[\mathbf{a}_k\mathbf{b}^k\right] = \left[a^1_k b^k_1, \dots, a^N_k b^k_N\right] \quad (17)$$

where $a^1_k b^k_1 + \dots + a^N_k b^k_N = 1$. Values of $a^i_k b^k_i$ close to unity indicate that the $i-th$ variable is strongly connected to the $k-th$ CSP mode. The non negligible values of the CSP Pointer for the 8 fast modes are displayed on Table II, at $t = 150min$; a point in time where all these modes are considered exhausted. It is shown that the 1^{st} mode points to BPG, the 2^{nd} mode points to GAP, the 3^{rd} mode points to both AMP and ADP, the 4^{th} mode points to PEP, the 5^{th} mode points to $F6P$, the 6^{th} mode points to $NADH$ and to a lesser degree to NAD^+, the 7^{th} mode points to $DHAP$ and the 8^{th} mode points to ACA; all these variables related the most to the fast dynamics of the problem.

Experience shows that when the CSP Pointer identifies a single variable (as in all, except the 3^{rd} and 6^{th}, modes), the related constraint, Eqs. (16), resembles a quasi steady state approximation (QSSA), while when more than one variable are identified the constraint resembles a partial equilibrium approximation (PEA) [30].

TABLE II

THE CSP POINTER FOR THE 8 FASTEST MODES ($t = 150min$)

	1	2	3	4	5	6	7	8
BPG	**0.99**							
GAP		**0.93**		0.03			0.03	
AMP			**0.53**	-0.01		0.02		
PEP		0.03		**0.94**		0.02		
$F6P$					**0.90**			
$NADH$				0.01		**0.58**	0.09	
$DHAP$		0.01				0.10	**0.74**	
ACA						0.01	0.02	**0.96**
Clc								
$EtOH$								
Glc_x								
ATP			0.05					
$G6P$					0.09			
ADP			**0.41**			0.01		
FBP		0.01				0.03	0.10	
NAD^+						**0.21**	0.01	0.02
Pyr								
$EtOH_x$								
$Glyc$								
$Glyc_x$								
ACA_x								0.01
CN^-_x								

This situation can be clarified by noting that in each of Eqs. (16) only a relatively small number of reactions participate in the occurring cancellations. These reactions can be identified with the CSP Participation Index [26]-[27], [31]:

$$P^k_i = \frac{q^k_i R^i}{\sum^{24}_{j=1}|q^k_{jf}R^{jf}| + \sum^{24}_{s=1}|q^k_{jb}R^{jb}|} \quad (18)$$

where k denotes the $k-th$ of the Eqs. (16), i denotes the forward or backward direction of the 24 reactions considered here, and by definition $P^k_1 + \dots + P^k_{48} \approx 0$ and $|P^k_1| + \dots + |P^k_{48}| = 1$. As a result, a relatively large value of P^k_i indicates a large contribution of the $i-th$ reaction to the $k-th$ constrain. Consider for example the 3^{rd} mode, for which the CSP pointer identifies AMP and ADP as variables related to a possible PEA. Using the CSP Participation Index and considering terms that produce $|P^3_i| > 0.02$, the amplitude of the mode at t=150min simplifies to:

$$f^3 = q^3_{9f}R^{9f} + q^3_{24f}R^{24f} + q^3_{9b}R^{9b} + q^3_{24b}R^{24b} \approx 0 \quad (19)$$

the RHS of which equals $0.76\ 10^{-2}$ with one $\mathbf{b}^r$-refinement and $0.44\ 10^{-4}$ with two. The Participation Indices are:

$$P^3_{9f} = 0.08 \quad P^3_{24f} = -0.40 \quad P^3_{9b} = -0.06 \quad P^3_{24b} = 0.40$$

These findings suggest that the relation $f^3 \approx 0$, being one among the eight describing the manifold, is indeed related to the equilibration of reaction 24, which involves both the pointed variables AMP and ADP. However, additional reactions have a smaller but significant influence, notably reaction 9 which involves ADP. The influence of this reaction on the shape of the manifold is displayed in Fig. 10, where $[AMP]$ vs $[Glc]$ is shown, computed with the original rate R^{9f} and a perturbed one $1.05 * R^{9f}$.

It is shown that a 5% perturbation in a term contributing 8% percent in the occurring cancellations inside $f^3 \approx 0$ produces an equivalent response of $O(0.4\%)$ in displacing the manifold.

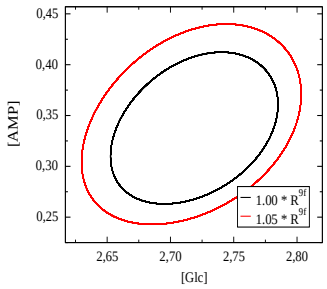

Fig. 10. The evolution in the phase space of AMP using both the original and the perturbed rate R^{9f}.

VI. Conclusions

Using a glycolysis model, a first demonstration was provided on how useful the analysis of a complex and stiff mathematical system can be if its fast and slow dynamics are examined separately.

Here only the fast dynamics, which are responsible for the development of the manifold, were discussed. Along similar lines can be discussed the slow dynamics which are responsible for the motion on the manifold.

References

[1] Z. Szallasi, J. Stelling, V. Periwal, *System Modeling in Cellular Biology: from Concepts to Nuts and Bolts*, MIT Press, Boston, 2006.

[2] R. Steuer, "Computational approaches to the topology, stability and dynamics of metabolic networks", *Phytochemistry*, vol. 68, 2007, pp 2139-2151.

[3] K. Smallbone, E. Simeonidis, D.S. Broomhead, D.B. Kell, "Something from nothing: bridging the gap between constraint-based and kinetic modelling", *FEBS J.*, vol 274, 2007, 5576-5585.

[4] W. Liebermeister, U. Baur, E. Klipp, "Biochemical network models simplified by balanced truncation", *FEBS J.*, vol 272, 2005, 4034-4043.

[5] J. Zobeley, D. Lebiedz, J. Kammerer, A. Ishmurzin, U. Kummer, "A new time-dependent complexity reduction method for biochemical systems", *Trans. Comput. Systems Biology I*, Springer Verlag, Berlin Germany, 2005, pp 90-110.

[6] D.A. Goussis, H.N. Najm, "Model Reduction and Physical Understanding of Slowly Oscillating Processes: the Circadian Cycle", *SIAM Multiscale Model. Simul.*, vol. 5, 2006, pp 1297-1332.

[7] A. Lovrics, A. Csikasz-Nagy, I.G. Zsely, J. Zador, T. Turanyi, B. Novak, "Time scale and dimension analysis of a budding yeast cell cycle model", *BMC Bioinformatics*, vol. 7, 2006, art.no. 494.

[8] S. Dano, M.F. Madsen, H. Schmidt, G. Cedersund, "Reduction of a biochemical model with preservation of its basic dynamic properties", *FEBS J.*, vol. 273, 2006, pp 4862-4877.

[9] G.Q. Dong, L. Jakobowski, M.A.J. Iafolla, D.R. McMillen, "Simplification of Stochastic Chemical Reaction Models with Fast and Slow Dynamics", *J. Biol. Phys.*, vol 33, 2007, 67-95.

[10] H. Schmidt, M.F. Madsen, S. Dano, G. Gedersund, "Complexity reduction of biochemical rate expressions", *Bioinformatics*, vol. 24, 2008, pp 848-854.

[11] S.R. Taylor, F.J. Doyle III, L.R. Petzold, "Oscillator Model Reduction Preserving the Phase Response: Application to the Circadian Clock", *Bio[hysical J.*, vol. 95, 2008, pp.

[12] C. W. Gear, *Numerical Initial Value Problems in Ordinary Differential Equations*, PrenticeHall, Englewood Cliffs, NJ, 1971.

[13] N. Fenichel, "Geometric Singular Perturbation Theory for Ordinary Differential Equations", *J. Diff. Eqs.*, vol 31, 1971, pp 53-98.

[14] P. Constantin, C. Foias, B. Nicolaenko, R. Temam, *Integral Manifolds and Inertial Manifolds for Dissipative Partial Differential Equations*, Appl. Math. Sci. 70, Springer-Verlag, New York, 1989.

[15] S.H. Lam, D.A. Goussis, "Understanding complex chemical kinetics with computational singular perturbation", *Proc. of the Comb. Inst.*, vol. 22, 1988, pp 931-941.

[16] S.H. Lam, D. A. Goussis, "Conventional asymptotics and computational singular perturbation for simplified kinetics modeling", in *Reduced Kinetic Mechanisms and Asymptotic Approximations for Methane-Air Flames*, Springer Lecture Notes 384, M. O. Smooke, ed., Springer, Berlin, 1991, pp. 227–242.

[17] U. Maas, S.B. Pope, "Simplifying Chemical Kinetics - Intristic Low Dimensional Manifolds in Composition Space", *Combust. Flame*, vol. 88, 1992, pp 239-264.

[18] U. Maas, S.B. Pope, "Implementation of Simplified Chemical Kinetics Based on Intrinsic Low Dimensional Manifolds", *Proc. of the Combustion Institute*, vol. 24, 1992, pp 103-112.

[19] C.W. Gear, I.G. Kevrekidis, "Constraint-defined manifolds: A legacy code approach to low-dimensional computation", *J. Scientific Computing*, vol. 25, 2005, pp 17-28

[20] S.J. Fraser, "The steady state and equilibrium approximations: a geometrical picture", *J. Chem. Phys.*, vol. 88, 1988, pp 4732-4738.

[21] M.R. Roussel, S.J. Fraser, "Geometry of the steady-state approximation: perturbation and accelerated convergence methods", *J. Chem. Phys.*, vol. 93, 1990, pp 1072-1081.

[22] H.G. Kaper, T.J., Kaper, "Asymptotic Analysis of two Reduction Methods for Systems of Chemical Reactions", *Physica D*, vol. 165, 2002, pp 66-93.

[23] A. Zagaris, H.G. Kaper, T.J., Kaper, "Two perspectives on reduction of ordinary differential equations", *Mathematische Nachrichten*, vol. 278, 2005, pp 1629-1642.

[24] F. Hynne, S. Dano and P.G. Sorensen, "Full-scale model in Saccharomyces cerevisiae", *Biophysical Chemistry*, vol. 94, 2001, pp 121-163.

[25] M.F. Madsen, S. Dano, P.G. Sorensen, "On the mechanisms of glycolytic oscillations in yeast", *FEBS J.*, vol 272, 2005, pp 2648-2660.

[26] S.H. Lam, "Using CSP to Understand Complex Chemical Kinetics", *Combust. Sci. Tech.*, vol. 89, 1993, 375-404.

[27] S.H. Lam, D.A. Goussis, "The CSP method for simplifying kinetics", *International Journal of Chemical Kinetics*, vol. 26, 1994, pp 461-486.

[28] A. Zagaris, H.G. Kaper, T.J. Kaper, "Fast and slow dynamics for the computational singular perturbation method", *SIAM Multiscale Model. Simul.*, vol. 2, 2004, pp 613-638.

[29] M. Valorani, H. N. Najm, D. A. Goussis, "Higher order corrections in the approximation of low dimensional manifolds and the construction of simplified problems with the CSP method", *J. Comput. Phys.*, vol. 209, 2005, 754–786.

[30] D.A. Goussis, M. Valorani, "An efficient iterative algorithm for the approximation of the fast and slow dynamics of stiff systems", *J. Comput. Phys.*, vol. 214, 2006, pp 316-346.

[31] D.A. Goussis, S.H. Lam, "A Study of Homogeneous Methanol Oxidation Kinetic Using CSP", *Proc. Comb. Inst.*, vol. 24, 1992, pp 113-120.

[32] M. Valorani, D. A. Goussis, F. Creta, H. N. Najm, "CSP analysis of a transient flame-vortex interaction: time scales and manifolds", *Combust. Flame*, vol. 134, 2003, 35–53.